Actuator Disc Modelling for Helicopter Rotors

Frédéric Le Chuiton
DLR – Institute of Aerodynamics and Flow Technology
Braunschweig, Germany

Abstract

The helicopter project CHANCE contains, among other developments, the quasi-steady approximation to modelling rotors with actuator discs. This reduces the cost of an unsteady simulation down to a stationary one. In testing existing approaches in the literature, the source term implementation proved to perform best especially in forward flight: source terms located on the disc bottom side impart impulse and energy to the fluid. These are obtained from a loose coupling between two DLR codes: the flow solver FLOWer and the rotor code S4. The latter provides a rotor map, a radial and azimuthal force distribution, to the former converting it to the actuator disc map (source terms). Low velocities are accounted for using preconditioning and a more flexible Chimera approach can be used. The actuator disc feature has been developed in a parallel framework for shorter turn-around times.

Capturing the fuselage/disc interaction using the Chimera capability is demonstrated on the HELIFUSE C1 configuration. Next the BO-105 fuselage is used to validate the source term approach by means of a uniform pressure jump. The potential disturbance appears clearly on the disc inflow and pressures on the top centreline match with experimental points. Last, the Dauphin 365N configuration has been used to assess the non-uniform actuator disc. It is checked that previous ONERAresults are correctly reproduced with a map provided by ONERA. An actuator disc map derived from S4 is used for further investigation. In particular it is shown that the vorticity field is particularly well captured.

Nomenclature

Latin Characters

A	rotor area
c	celerity of sound
C_T	thrust coefficient
$\bar{\bar{F}}$	flux tensor
$F(r,\psi)$	local force normal to a blade element
$\vec{f}$	force distribution over the disc
$k^{(2)}$	2nd order dissipation coefficient
$k^{(4)}$	4th order dissipation coefficient
H	total (stagnation) enthalpy
M_∞	upstream Mach-number
M_{tip}	tip radius Mach-number
$\vec{n}$	a unit vector
P_P	preconditioning matrix in U_P
p	static pressure
$\bar{\bar{Q}}_S$	boundary stress tensor
R	rotor tip radius
r	radius of a point on the disc
Re_∞	Reynolds-number per metre (m^{-1})
T	rotor thrust
U_C	vector of conservative variables
U_P	vector of variables for preconditioning
V	cell volume
$\vec{v}$	velocity vector
v_n	$= \vec{v}\cdot\vec{n}$ normal velocity component
$\vec{v}_t$	$= \vec{v} - v_n\vec{n}$ tangential velocity component
w	one-dimensional characteristic variable

Greek Characters

α	angle of incidence
α_{shaft}	shaft angle of the disc
Γ_P	preconditioning matrix in U_C
γ	ratio of specific heats
ϵ	sign function
θ	relaxation coefficient
λ	eigenvalue
μ	advance ratio of the helicopter
ρ	fluid density
σ	spectral radius of a matrix
ψ	azimuth of a point on the disc
ω	rotor rotational speed

Introduction

The French-German helicopter programme Complete Helicopter AdvaNced Computational Environment (CHANCE) [31] has been started mid 1998 and runs for six years. Research establishments on both sides of the river Rhine (ONERA, DLR and IAG-University of Stuttgart) are committed, in the frame of an integrated team, to develop numerical methods for simulating the flow-field around complete helicopter configurations and to supply the French-German company Eurocopter with the resulting CFD codes: elsA from ONERAand FLOWer from DLR.

The project CHANCE can be seen as made of three main point of views: a steady state context for isolated rotors in hover and isolated fuselages, then a so-called quasi-steady approach for fuselages with rotors modelled as actuator discs and finally the pure unsteady procedure for isolated rotors in forward flight and complete helicopters. The main document of the project defines a list of algorithmic development work packages, out of which one or more may be combined so as to run a numerical simulation in the frame of one of the three aforementioned backgrounds.

Quasi-steady computations are meant to combine a substantial set of these algorithmic features. First, time-averaged interactional aerodynamics between the fuselage and the rotors are to be modelled by means of actuator discs. Then integration of the Navier-Stokes equations is to be augmented by turbulence modelling using 2-transport equation turbulence models and also by transition prescription. Next, in order to account for typical flight speeds of helicopters, use of the low-velocity preconditioning technique is foreseen. It has been further decided to make use of the Chimera technique so as to reach high flexibility during mesh generation of multi-block structured grids. In particular, a special grid system for the actuator disc can be generated and then superimposed on a pre-existing fuselage mesh, thus on the one hand saving remeshing costs and on the other hand allowing studying different positions and orientations of the disc. Finally, since large applications are to be run by industrial partners on clusters of workstations or even PCs, the complete numerical procedure must be parallelised.

This article aims at presenting the state of development at DLR of the quasi-steady approach as explained above. Although both capabilities transition prescription and Chimera were available, transition setting will be not reported here and Chimera only briefly mentioned.

Base Numerics

The base CFD tool for this study is the code FLOWer developed at DLR over the past ten years [12, 32] and designed to handle multi-block structured meshes. The unsteady Reynolds-averaged Navier-Stokes equations are discretised in space using one of the two flavours of the finite volume approach at hand: either cell-vertex (making use of the supercell concept) or cell-centred, whereby flow unknowns are located either at grid nodes or at cell centres respectively.

Spatial discretisations of convection fluxes result from the application of either the Jameson scheme (central fluxes plus second and fourth order dissipation) or the upwind AUSM/Van Leer scheme [14], while viscous fluxes are centrally discretised, and time integration is carried out by means of a 5-stage Runge-Kutta cycle. Usual techniques: local time-stepping, implicit residual smoothing and multigrid cycling are then used to enhance the convergence properties.

Beyond this numerics basis, FLOWer can also handle low-velocities by means of preconditioning [19], possesses a full implementation of Chimera features [27] (no hierarchical mesh dependencies) and has further unsteady developments [17]: an implicit time integration using the dual-time stepping method by Jameson, an extension of the equation formulation to moving and deforming meshes and a geometry conservation law.

The Reynolds-stress tensor is modelled using Boussinesq's assumption and the resulting eddy viscosity in turn can be calculated by the algebraic Baldwin-Lomax model or in integrating the 1-transport equation Spalart-Allmaras model or a series of 2-transport equation models, the famoust of which is the Wilcox $k - \omega$ model. Convection fluxes of the turbulence equations are discretised by a first order accurate Roe scheme and turbulence variables are integrated in time by means of a single grid implicit DDADI (diagonal dominant alternating direction implicit) scheme [25].

Boundary conditions for the conservative and turbulence variables follow the one-dimensional characteristics theory on far-field boundaries, mirror the variables on symmetry planes and set a no-slip condition on solid bodies.

Finally, the code has been parallelised [15] making use of the MPI framework. All MPI calls are actually encapsulated in the library CLIC3D that entirely cares for communications.

Actuator Disc

Reducing the complexity of the simulation of the unsteady flow of a rotating machine can be reached by replacing the rotary wing or thrust generator with a physical simplification. Thereby a solid infinitely thin annular zone is substituted to the rotor along the blade path and dynamics effects are somehow modelled and applied to the medium as it flows through the disc.

A first level of approximation consists in retaining an unsteady framework and projecting the actual blades onto the disc, so that only their traces act on the fluid as they rotate around the machine axis. This has recently been tried in the field of helicopters by Boyd & Barnwell [20] and Tadghighi [29]. On the one hand, although geometrically simplified, the cost of the numerical simulation is that of an unsteady one, but on the other hand at least the first harmonic of unsteady phenomena is captured.

The next step is based on a steady-state assumption, whereby the complete azimuthal range of the disc is filled up with blades and the force distribution is scaled according to the target thrust. In this case, the unsteady description is lost, but computational costs are drastically reduced to one steady-state simulation. A vast majority of literature references follow this approach, including the present work.

Modelling

Modelling a rotating machine necessitates taking the type of application into account: indeed each case appears to have its own natural set of descriptive variables, in fact very much guided either by quantities that can be measured or by other modelling approaches.

Actuator discs for fans of turbojet engines make usually use of the performance characteristics of the blade row: relative outlet flow angle and entropy rise [18] or total pressure and total temperature ratios and swirl

[22] or else total pressure ratio and adiabatic efficiency [23], usually as functions of the radius.

Propellers have been modelled either by their characteristics: total pressure and total temperature ratios and swirl in [2, 4], or by a force distribution supplied by an auxiliary code based either on the blade element theory or on a lifting line/vortex lattice method in [4, 10, 11].

As for helicopter rotors, since it is not possible to draw up characteristics in the sense of turbomachines, one relies either on a global (or even stripwise [1]) momentum approach or on a more refined blade element theory to describe the force distribution [7, 8, 13, 16, 20] or else on a lifting line/vortex lattice code [21, 26].

Implementation

The influence of solid bodies is felt in a numerical discretisation by means of boundary conditions and an actuator disc, as model of a solid actuating body, can be implemented in this way. From another point of view, the rotor is replaced by a zero-volume disc, the action of which is only effective on its surface. In this regard, the effect of the actuator disc can be seen as a boundary stress applied on the surface of a control volume, and this is reflected as a source term in the equations.

In the field of turbomachines, authors seem to well agree since they all use the boundary condition formulation. As for propellers and helicopter rotors, scientists are subdivided into two approximately equally populated groups: the boundary condition defenders and the source term supporters. In fact, it seems that internal flows are best served with the boundary condition approach, while external flows can stand both.

This distinction is actually not always very clear since formulations share sometimes common points or can even be transformed into one another. Anyway the following can be taken as a tentative classification and is based on what authors claim.

Boundary Condition In this framework, the actuator disc is first of all considered as being represented by the common surface between two or more grid blocks (more than one block may lie on one side of the disc).

Then two features can be traced as common basis in all related works [4, 7, 11, 13, 18, 22, 23].

The argument of propagation of characteristics is first invoked in order to determine the number of specified and extrapolated quantities on the boundary: one and four respectively on an outlet (outlet from the computational domain) and conversely four and one respectively on an inlet. It is here assumed that the throughflow remains subsonic, which represents the nominal conditions of almost all applications, except when a turbomachine blade row chokes [18]. In this context is to be also noted the interesting suggestion of Kim *et al.* [23] to use a modified Riemann problem so as to get boundary values.

Second, making the implementation mass conservative is compulsory, which is enforced in assigning the local mass flow to the upstream propagating characteristic. On the inlet boundary (downstream side), the mass flow is extrapolated from the interior of the block, while on the outlet boundary (upstream side) the mass flow is set equal to that of the other side.

Some implementation details are, in the field of turbomachine fans, worth noting. Joo & Hynes [18] suggested in order to have a treatment more suitable to unsteady effects simply to exchange the values of the mass flow, radial velocity and rothalpy between both sides of the disc. This is to be connected to the first stage of the source term strategy explained further down. Wilhelm [22] observed convergence problems when specifying mass flow continuity on the upstream side. This has been relieved, first, in extrapolating now the mass flow too and, second, in substituting an artificial pressure condition to the mass flow specification: the relative difference in mass flows between both sides is used to determine an artificial pressure correction, which is then added to the pressure. This correction is further relaxed by means of a parameter and disappears upon convergence since both mass flows are then equal.

As regards propeller applications, Yu *et al.* [4] and Lötstedt [11] use the same formulation, which looks very much like a source term approach: the convective flux on the downstream side is set equal to that on the upstream side and is augmented by force and work terms to the impulse and energy components. Flow variables then follow from the application of the two principles mentioned above.

Fejtek & Roberts [7] in a compressible fluid framework and Chaffin & Berry [13] in an incompressible one, dealing with tilt-rotors or helicopter rotors respectively, apply mass flow continuity and extrapolation of variables, and specify jumps in pressure and tangential velocity.

It is finally to be mentioned that many authors have taken into account the possibility of a reverse flow through the actuator disc, that is: from the theoretically downstream side to the theoretically upstream side. This is particularly important for helicopter rotors in forward flight where the flow is directed from bottom to top on the very front part of the disc and is to remain so upon convergence.

At last is to be noted the successful application of the boundary condition formulation of the actuator disc concept to the simulation of lattice wings of missiles by Reisch [24] and Reynier [28].

Source Terms Considering an actuator disc the other way round, no longer as a boundary condition representing an obstacle (though permeable: mass flux conservation) to the fluid but instead as a mere throughflow condition between blocks, proves much simpler. In this case, flow values are first exchanged between both sides of the disc like for any other inter-block connection, then a flux common to both sides is calculated using the normal numerical scheme and stencil, and finally a force is added to the impulse equation and, in case the compressible conservation equations are solved, its associated work to the energy equation.

Such an implementation seems to appear first in Whitfield & Jameson [2] for propeller/wing interaction problems: the downstream side of the disc is now the place where source terms are added to the residuals of the abutting cells. Making use of Gauss' divergence theorem, the formal equivalence between volume and surface source terms is illustrated, where the latter are of course to be preferred since an actuator disc is a two-dimensional entity. Schipholt *et al.* [10] went back on this formulation too.

As regards helicopter rotors, Rajagopalan and coworkers [8, 9] early applied a source term approach in an incompressible flow simulation code. They developed an original, and up to now unique, method to detect the cells where the actuator disc source terms should be assigned to. Instead of considering the disc as a common surface between two blocks, cells lying on the rotor blade path are searched for and retained for the source term addition. This allows greater flexibility as far as mesh generation is concerned, though at the price of an additional algorithm. Other authors [16, 21, 26, 29] use the traditional cut condition technique. At ONERA, an original formulation has been developed by Bettschart [21]: a special flux for the cell-faces lying on the disc was designed using the one-dimensional characteristic theory, whereby the two aforementioned guiding ideas were enforced. Although referred to as a boundary condition by its author, this approach is to be classified as a source term method.

An early work by Rajagopalan [5] has also made use of the source term formulation for windmill turbines.

Present Work In the course of our development of the actuator disc option in FLOWer several implementations have been tried that all but the last proved more or less unsatisfactory.

Many of them used as a first step an extrapolation of the variables from the interior of the grid blocks onto the boundary representing the actuator disc. Because of transient or persisting numerical oscillations in the close vicinity of the disc, a first order extrapolation proved more robust than a second order one. Anyway we are provided with flow values on both the top/upper and bottom/lower sides denoted with "u" and "l"-subscripts respectively. The "top/upper side" refers to the side, which the thrust vector points to, and the "bottom/lower side" to the other one. Further let flow values meant as located on the boundary/disc itself be subscripted with a "b".

A simple actuator disc model, namely a uniform pressure jump, has been used throughout our numerical developements, thus uncoupling modelling and numerical issues. A more refined model was then used in the final computations.

• *Momentum Formulation – Boundary Condition on Variables.* First of all, a boundary condition in the sense of [7, 13] had been tested using the cell-vertex discretisation: since flow values are assigned on grid nodes, boundary variables are here updated and further used to calculate fluxes. The downstream condition then read

$$\begin{cases} \vec{v}_{t_b} = \vec{v}_{t_u} \\ p_b = p_u + \Delta p \\ H_b = H_u + \frac{\gamma}{\gamma-1}\frac{\Delta p}{\rho_u} \\ (\rho v_n)_b = (\rho v_n)_l \end{cases}$$

while two flavours of the upper condition had been tried, the second of which retained the artificial pressure correction suggested in [22]

$$(a)\begin{cases} \rho_b = \rho_u \\ (\rho\vec{v}_t)_b = (\rho\vec{v}_t)_u \\ p_b = p_u \\ (\rho v_n)_b = (\rho v_n)_l \end{cases} \qquad (b)\begin{cases} \rho_b = \rho_u \\ (\rho\vec{v}_t)_b = (\rho\vec{v}_t)_u \\ p_b = p_u + \delta p \\ (\rho v_n)_b = (\rho v_n)_u \end{cases}$$

where ρ, p and H denote the fluid density, the static pressure and the total enthalpy respectively, $v_n = \vec{v}\cdot\vec{n}$ and $\vec{v}_t = \vec{v} - v_n\vec{n}$ further refer to the velocity components normal and tangential to the disc ($\vec{v}$ is the velocity and $\vec{n}$ a unit vector normal to the disc). The pressure jump Δp represents the user-supplied condition and the artificial pressure correction δp reads

$$\delta p = \theta\,\frac{(\rho v_n)_u - (\rho v_n)_l}{(\rho v_n)_l}\,.$$

When the flow is directed from top to bottom, this correction modifies the upper pressure so as to drive the upper mass flux towards the lower one. This worked correctly in forward flight giving converged solutions (up to six orders of magnitude) with a reversed flow portion on the front. Nevertheless the right hand side is not homogeneous to a pressure, which might look strange to an expert eye. In fact non-dimensionalised pressures lie around unity as well as the suggested mass flux fraction; this did not hinder the numerics. Finally θ is a relaxation parameter, the value of which ranged between 0.1 and 0.5 for upstream Mach-numbers between 0.02 and 0.2 respectively.

With this formulation of the actuator disc, Froude's one-dimensional momentum theory could be successfully recovered: the actuator disc was able in a propeller-like mode to deliver the proper contraction ratio of the slipstream and the correct induced velocity within one percent tolerance. It has even been possible to compute a fuselage/actuator disc forward flight case with Chimera grids (see further down the section on results).

Unfortunately, serious robustness problems occurred and this implementation had to be dropped. Reducing the coefficient of the fourth order artificial dissipation was hardly possible and setting the height of the first cell above and below the disc to less than one percent of the tip radius led automatically to run failure. Last, it has never been possible to converge down to machine precision for simple isolated actuator disc cases.

• *Characteristic Formulation – Boundary Condition on Variables.* The second attempt, still in cell-vertex, is the "boundary condition on variables"-variant of the procedure suggested by Bettschart and Brézillon [21, 26], who adapted the one-dimensional characteristic formulation of boundary conditions, originally developed by Whitfield & Janus [3], to the actuator disc.

Following Whitfield, the Euler system of equations in quasi-linear form, when linearised around a reference state (subscript "o") and projected along a direction given by a unit vector $\vec{n}$, can be transformed to an uncoupled system of equations for the one-dimensional characteristic variables w, each associated to its eigenvalue λ.

$$\left\{\begin{array}{l} \lambda^o = v_{n_o} \\ \lambda^+ = v_{n_o} + c_o \\ \lambda^- = v_{n_o} - c_o \end{array}\right. \qquad \left\{\begin{array}{l} w^o = (\rho - \frac{p}{c_o^2})\vec{n} + \vec{v} \times \vec{n} \\ w^+ = \frac{p}{\rho_o c_o} + v_n \\ w^- = \frac{p}{\rho_o c_o} - v_n \end{array}\right.$$

In our case, averaging upper and lower states provides the reference state considered as located on the disc. Next let $\vec{n}$ be the unit vector normal to the disc and pointing to the upper side. Then assuming an always subsonic normal flow, the eigenvalues are ordered as follows: λ^o points either downwards (sign $\epsilon = -1$) or upwards (sign $\epsilon = +1$), and λ^+ and λ^- always point upwards and downwards respectively. Using these directions of propagation, assigning characteristic variables on the disc would read

$$\left\{\begin{array}{l} w_b^o = \frac{\epsilon+1}{2} w_l^o + \frac{\epsilon-1}{2} w_u^o \\ w_b^+ = w_l^+ \\ w_b^- = w_u^- \end{array}\right.$$

Instead and following the ever enforced association of the mass flux to the upstream propagating characteristic, one specifies on the disc boundary

$$\begin{array}{cc} (\epsilon = +1) & (\epsilon = -1) \\ \left\{\begin{array}{rl} w_b^o & = w_l^o \\ w_b^+ & = w_l^+ \\ (\rho v_n)_b & = (\rho v_n)_u \end{array}\right. & \left\{\begin{array}{rl} w_b^o & = w_u^o \\ (\rho v_n)_b & = (\rho v_n)_l \\ w_b^- & = w_u^- \end{array}\right. \end{array}$$

These relations yield a second order equation for the normal velocity component v_{n_b}, the minimum root of which is then taken as the solution. The rest of the boundary variables (ρ_b, p_b and $\vec{v}_{t_b}$) follows from simple algebra. This common boundary state is then assigned to both sides of the disc and the pressure on the bottom side is augmented by the user-supplied pressure jump Δp.

Whatever nice this formulation may look, unfortunately and surprisingly no major improvements were achieved concerning sensitivities on the fourth order dissipation coefficient and on the height of the first cell. Axial flight was still correctly captured when compared to Froude's theory, but now forward flight conditions experienced strong stability problems, which were traced back to the inversion line lying on the front of the disc, where the fluid first flows from bottom to top and then from top to bottom. Moreover and contrary to the previous implementation, the characteristic formulation worked better in conjunction with the upwind AUSM/Van Leer scheme than with the central Jameson's scheme.

• *Characteristic Formulation – Boundary Condition on Fluxes.* It is here necessary to make a distinction between the base numerical scheme for convection fluxes used everywhere in the core of the flow field (in cell-vertex: Jameson, and in cell-centred: either Jameson or AUSM/Van Leer) and the convection flux formula used on the actuator disc boundary. The former, when calculated by the Jameson scheme, is made of two subparts: a so-called centred flux (as appearing in the equations) and a dissipation flux (for the sake of numerical stability), while the upwind convection flux consists in one single formula.

As the base scheme was first set to Jameson, the flux on the disc was chosen to be Jameson-like: a combination of a centred flux and of a dissipation flux. The actual form of these two fluxes had then to be determined.

The characteristic boundary state, as obtained in the previous subsection, was in this case directly used to calculate the centred flux on cell-faces lying on the disc, instead of a mere average of neighbouring cells like in the Jameson's scheme. Doing so in cell-vertex, flow values on the boundary result from an update using the corresponding residuals. Therefore we refer to this approach as a boundary condition on fluxes, since the first step of the boundary treatment specifies fluxes and not variables. With the cell-centred discretisation, as flow values on the boundary are not solved by the algorithm, one cannot but use boundary conditions on fluxes.

Besides it has been investigated, in cell-vertex and cell-centred, whether a special version of the artificial dissipation operator should be applied on the disc (like for walls or far-field boundaries) or not (discretisation stencil extending through the disc as if there were none).

Alone swapping from "boundary condition on variables" to "boundary condition on fluxes" cleared up almost all difficulties: no lower bound any more on the height of the first cell, no more restriction on the fourth order dissipation coefficient. Climb cases were again perfectly captured but unfortunately, in forward flight, instabilities along the line of reversed flow held against any attempt to tune the base scheme, thus causing convergence to level off, unless the CFL number was screwed down to unacceptably small values or the artificial dissipation to unacceptably high ones.

As a final try in cell-centred, the base scheme was set to the upwind AUSM/Van Leer scheme and the boundary flux was derived using only the centred flux mentioned above.

This improved the convergence history a little but did not rescue the situation.

• *Source Term Formulation.* Simulations routinely run in the industry with FLOWer make use of the Jameson's scheme. Hence it was highly important to get it running with the actuator disc option.

With this last formulation the disc boundary is nothing more than a usual interface between two or more blocks of the multi-block mesh. That is: fluxes on the disc use exactly the same stencil and formulæ as for the base numerical scheme and actuator disc source terms are simply added to residuals of the cells lying underneath. For example, for a cell V with surface ∂V abutting the disc on the bottom:

$$\frac{\partial}{\partial t}\int_V U_C\, dV + \oint_{\partial V} \bar{\bar{F}}(U_C)\cdot\vec{n}\, dS = \oint_{\partial V} \bar{\bar{Q}}_S \cdot \vec{n}\, dS$$

where U_C is the vector of conservative variables, $\bar{\bar{F}}$ the flux tensor and $\bar{\bar{Q}}_S$ the boundary stress tensor. Further we have

$$\bar{\bar{Q}}_S \cdot \vec{n} = \begin{pmatrix} 0 \\ \vec{f} \\ \vec{f}\cdot\vec{v} \end{pmatrix} \qquad \vec{f} = \vec{f}(r,\psi)$$

with $\vec{f}$ the local force density being non-zero only on the cell-face on the lower side of the disc, and being generally written as a function of the rotor local coordinates: radius r and azimuth angle ψ.

The former approach (characteristic formulation and boundary condition on fluxes) reduces exactly to the present one when the complete convective flux on the boundary is chosen to be the same as the one used in the core of the flow-field, that is: not only flux formulæ are identical but also their arguments.

This last implementation allowed this time all computations to converge properly, relieving all robustness problems. Now since the base numerical scheme is applied through the disc, the flow-field in its close vicinity follows directly from the behaviour of this base scheme, which in turn is influenced by the presence of source terms. These act like a pressure jump, the strength of which depends on each coordinate direction. Therefrom nearby the disc, the Jameson's scheme delivers oscillations, while the upwind scheme causes less wiggles. In contrast, as observed in the previous subsection, a characteristic flux on the disc removes any fluctuation but at the price of no convergence. Additionally, it has been observed that the central Jameson's scheme now exhibits a smoother convergence than the upwind AUSM/Van Leer scheme, whereas it had been exactly the opposite up to this source term formulation. The present author has thus far no explanation for this behaviour, but still remains confident in the combination upwind scheme/actuator disc source terms since successful applications have been reported in [16] with a fifth order accurate Roe scheme and in [29] with an even more accurate, sixth order, symmetric total variation diminishing Roe scheme.

The compromise reached thus far seems reasonable to the author: satisfactory convergence at the expense of unimportant wiggles around the disc. Remember, these are numerical oscillations that extend over few cells, thus kept far away from the helicopter fuselage. In the end, the actuator disc downwash and its influence on rear control surfaces are of importance and not the disc itself, which is anyway only a model of the rotor. Hence all computational results presented in this paper make use of this source term formulation (except for the Chimera demonstration run).

Coupling With a Rotor Simulation Code

The strategy here adopted represents a "loose coupling": output data of a rotor simulation code are read in into FLOWer, further transformed so as to initialise the actuator disc source terms and the CFD simulation is run as a usual one. Thus no feedback of the fuselage potential disturbance takes place on the rotor inflow. As a consequence, the rotor may not be trimmed any more, as it is when computed on its own. A simple workaround would consist in periodically restarting the procedure, whereby inflow velocities are given back from the CFD code to the rotor code, until no more changes in the rotor controls occur. No built-in trim-procedure like in [7, 13, 29] has been used.

The rotor code retained here is named S4 and developed at DLR by van der Wall [6]. It is based on blade element theory making use of two-dimensional aerofoil tables and a vortex lattice method allowing to relax the rotor wake to equilibrium. The interested reader is referred to the reference cited above.

The rotor code S4 supplies a data file, here referred to as the *rotor map*, containing several quantities as functions of the radius r and azimuth angle ψ in the "isolated rotor frame" (X,Y,Z) as depicted in figure 1. This file is read in into FLOWer and further worked on in order to get the distribution of source terms, here termed *actuator disc map*. In particular, the local force $F(r,\psi)$ normal to each blade element is first projected in the (X,Y,Z) reference frame, then divided by the blade element area so as to obtain a local force density. This force density distribution is then interpolated onto the mesh of the actuator disc, taking also into account an azimuth shift due to a possible side-slip angle of the upstream flow; it is finally transformed to the global reference frame (X_o,Y_o,Z_o) as displayed in figure 2 and yields the expected source terms $\vec{f}=(f_x,f_y,f_z)$.

Preconditioning

Typical helicopter flight conditions correspond to low subsonic velocities, for which an upstream Mach-number of 0.2 is most of the time an upper limit. Hence it was necessary to have the possibility to use the low-Mach number preconditioning technique, first, so that the artificial dissipation of the Jameson's scheme scales properly for all variables and, second, so that convergence not only of residuals but more importantly of the integral coefficients is enhanced.

The characteristic formulation of the actuator disc implementation is based on intrinsic properties of the underlying system of equations. Therefore such a formulation has to be adapted to the preconditioned system: in practice new formulæ for the eigenvalues, celerity of sound and characteristic variables must be used. The characteristic formulation accordingly modified has been tried unfortunately unsuccessfully and no much time was spent on it since we already made up our mind for the source term variant.

On the opposite, this source term formulation needs not be adapted since it acts precisely by means of source terms, and yields a preconditioning capable formulation for free. Consider a cell lying on the bottom side of the disc, with volume V and cell-faces identified with their surface area S and unit normal vector $\vec{n}$. Let also S_{AD} be the surface area of the cell-face lying on the disc. Then assuming Q_{AD} to be the actuator disc source term on S_{AD}, the preconditioning technique tells

$$V\frac{\partial U_C}{\partial t} + \frac{\partial U_C}{\partial U_P} \cdot \Gamma_P \cdot \left\{ \sum_{f\in\partial V} \left[\bar{\bar{F}}(U_C) \cdot \vec{n}\, S \right.\right. \\ \left.\left. + \Gamma_P^{-1} \cdot \sigma\Big(P_P A_P\Big) \frac{\partial^3 U_P}{\partial \vec{n}^3} \right]_f - Q_{AD} S_{AD} \right\} = 0$$

where the subscript "$_f$" denotes a summation over the six faces of the cell. U_C represents the conservative variables and U_P an appropriate set of variables for preconditioning. Additionally, A_P denotes the Jacobian matrix of the flux in U_P variables and P_P and Γ_P are the preconditioning matrices up to a change of variables. Finally $\partial^3/\partial\vec{n}^3$ represents a third order derivative in the running direction under the summation sign and $\sigma(\cdot)$ is the spectral radius of its matricial argument. Details are to be found in the work of Turkel *et al.* in [19].

Parallelisation

Parallel computing facilitates reducing turn-around times, an everlasting demand from users of CFD codes. Therefore the actuator disc option had to be properly inserted into the parallel framework of FLOWer: a master process cares about all input/output operations and distributes input data to all other processes. Of course, all processes share the computational load.

The actuator disc surface consists of several cut segments connecting blocks abutting on both top and bottom sides and these are distributed over the available processes. Hence in general one given process handles zero, one or more actuator disc cut segment. Adding source terms to residuals makes no difficulty as long as the right source terms are available on the right process. Hence parallelising the actuator disc feature was only a matter of pre-processing. In this context the master process reads in the rotor map, prepares them as explained above and distributes the resulting actuator disc map to all other processes. In this way, each process has the possibility to initialize the source terms required for the actuator disc cut segments that it manages. Distributing the actuator disc map to all processes, also where actually not needed, may look as a waste of memory, but proves in fact to be a reasonable compromise between simplicity of the implementation and memory overhead, that is anyway restricted to a very small two-dimensional entity in comparison to the complete grid.

Chimera Capability

Accounting for the actuator disc right away during generation of the fuselage mesh is non-trivial, all the more difficult as the disc lies close to the engine casing: additional topology and refinement constraints are to be managed. It is consequently much simpler to generate a separate grid for the isolated actuator disc and superimpose it on top of a pre-existing fuselage mesh. The position and orientation of the rotor can then be adapted and investigated.

An early Chimera inviscid demonstration computation had been done with the HELIFUSE C1 configuration combined with a disc and cast into a Cartesian background grid. The flight conditions were $M_\infty = 0.25$ and $\alpha = -6.7^o$ and a uniform actuator disc had been used with thrust coefficient $C_T = 0.007$. The integration was carried out with the Jameson's scheme without second order dissipation and with a relatively high fourth order dissipation coefficient $k^{(4)} = 1/32$ (momentum formulation with boundary condition on variables). Also, no multigrid could be used due to too poor an overlap on coarser grid levels. The CFL number was set to 4.

In figure 3 are depicted pressure contours and normal mass flow contours on the fuselage and actuator disc surface respectively. The fuselage potential disturbance can be clearly seen on the front part of the disc, thus validating the Chimera approach for interactional aerodynamics. No feedback from the disc on the fuselage can be detected since with this relatively high Mach number the disc downwash is directly swept away. Also to be seen on the disc are the traces of the vortices shed from the inner radius.

Results

As far as actuator disc modelling in CHANCE is concerned, two Eurocopter configurations have been retained as validation test-cases: the BO-105 and the Dauphin 365N.

The numerical settings of both cases have been as far as possible kept similar and correspond anyway to a usual way of running FLOWer. Important common features are: the cell-centred discretisation, the scheme of Jameson, the artificial dissipation coefficients of which were set to $k^{(2)} = 1/2$ and to $k^{(4)} = 1/64$; V-like multigrid cycles over three or two levels when running on the finest or second finest grid level respectively. The CFL-number was set to its default value of 7.5 for the BO-105 and to 5.5 for the Dauphin because of grid singularities. The low-velocity preconditioning has been switched on only for the Dauphin. No Chimera has been used since, in both cases, meshes with already existing actuator discs were available. Finally, the parallel implementation of the actuator disc feature has been validated but is not reported here for the sake of simplicity.

BO-105 Configuration

The BO-105 configuration is the main validation line of the CHANCE programme: applications range from the isolated fuselage, over fuselage with rotors as actuator discs and up to unsteady simulations of the complete fuselage with rotors, and as such has been first presented by Khier in [30].

The grid has been generated at DLR and contains approximately 11 million points distributed in 99 blocks, see figure 4 where only every other point on surfaces has been depicted. An O-block topology has been used around the fuselage, while an H-topology was retained around the disc, the hub of which has been neglected.

General flight conditions are given by the upstream Mach number M_∞, the angle of incidence α and the Reynolds number per metre $\mathrm{Re}_\infty = \rho_\infty V_\infty/\mu_\infty$. Specific rotor parametres are the tip Mach number $M_{\mathrm{tip}} = R\omega/c_\infty$, the thrust coefficient $C_T = T/\rho_\infty(R\omega)^2 A$ and advance ratio $\mu = V_\infty/R\omega$. Their numerical values are:

$$\begin{aligned} \alpha &= -0.66^o & M_{\mathrm{tip}} &= 0.638 \\ M_\infty &= 0.125 & C_T &= 0.006315 \\ \mathrm{Re}_\infty &= 2.91\ 10^6\ (\mathrm{m}^{-1}) & \mu &= 0.2 \end{aligned}$$

The rotor has been modelled by a uniform pressure jump calculated as $\Delta p = \rho_\infty c_\infty^2 M_{\mathrm{tip}}^2 C_T$.

Figure 5 displays the distribution of normalised total pressure along with streamlines in the symmetry plane, whereby it appears clearly that the fin and the stabilisers experience a totally different flow in comparison to an isolated fuselage simulation. The insert in the same picture shows the pressure distribution along the top centreline, where experimental points (hollow squares) are relatively well reproduced by the computation (solid line). However, modelling the hub and specifying a more realistic force distribution on the disc could further improve the agreement. In figure 6 are displayed surface distributions: pressure coefficient on the fuselage and normal velocity component on the disc. The blocking influence of the fuselage is to be seen on the front part of the disc where the inflow is reduced in comparison to the sides. Also to be noted are the thin zones on both sides where the fluid flows from bottom to top. More insight in the BO-105 test-cases can be found in [30].

Dauphin 365N Configuration

The Dauphin 365N configuration has been experimentally tested, meshed and computed at ONERA, see Brézillon [26] and references therein, and is part of the programme CHANCE. In this context, experimental data, a structured multi-block mesh and a ready-to-use actuator disc map have been made available to partners by ONERA.

The mesh of the Dauphin is displayed in figure 7 and is made of around 7 million points gathered in 94 blocks. The fuselage as well as the disc are embedded within O-topologies and the stabilisers and the fin within C-topologies. This grid was particularly designed to allow efficient vorticity convection, especially marginal vortices of the disc, and in respect thereof has proven to be of high quality.

Flight and rotor conditions are:

$$\begin{aligned} \alpha &= -3^o & M_{\mathrm{tip}} &= 0.294 \\ M_\infty &= 0.044 & C_T &= 0.006196 \\ \mathrm{Re}_\infty &= 1.07\ 10^6\ (\mathrm{m}^{-1}) & \mu &= 0.15 \end{aligned}$$

where the relatively small value of M_{tip} is due to the smaller tip radius of the wind tunnel model. The upstream flow makes with the disc an angle of $\alpha_{\mathrm{shaft}} = -7^o$.

First of all, validation runs have been carried out with and without actuator disc map (that from ONERA) and have been compared to computational results presented in [26]. On figure 8 are depicted pressure distributions along the top centreline: isolated fuselage above and fuselage with non-uniform actuator disc below. Experimental points are identified with circles and the computation with the solid line: good agreement has been reached notably thanks to the use of preconditioning. The presence of the rotor head, in both cases during the wind tunnel experiment, inevitably modifies the flow-field downstream of it, which is not reproduced here in the present simulations. Further comparisons have been done and show good global agreement with results given in the aforementioned reference, which the interested reader is referred to.

Next, a rotor map has been generated by S4 and used to assess the FLOWer/S4 coupling procedure. Another rotor, than the one of the ONERAexperiment, but flying with the same operating conditions (except for the trim law) has been retained in order to put into light to what extent the flow-fields produced by different rotors differ. To this end, the rotor retained is the ONERA7A rotor, the characteristics of which were then available in S4. Thereby, thrust coefficient, advance ratio, shaft angle have been kept identical while the rotor was run in rigid blade mode with a moment-free trim law. This is not meant as being a realistic simulation but only as input rotor map to FLOWer.

In figure 9 are displayed convergence histories of residuals and integral coefficients of a computation done on the second grid level, which allowed only two levels in a multigrid cycle. To be noted is the somewhat difficult transient phase between iterations 600 and 1600, that is attributed to the threefold conjunction of turbulence development, particularly in boundary layers, of the effect of a non-uniform rotor downwash and of mesh singularities. On this Dauphin mesh, this behaviour has been observed in all our non-uniform actuator disc computations, whatever the grid level used: finest or second finest and whatever the actuator disc map: ONERAmap or S4 map. However, as expected, running on the finest level, thus allowing three levels in the multigrid procedure, reduces significantly the iteration range over which oscillations occur. Further, with a uniform pressure jump over the disc, no convergence problem whatsoever appeared thus leaving no doubt about the origin of convergence wiggles.

Corresponding to the convergence mentioned above is now depicted in figure 10 the flow solution obtained on the second grid level (approximately 850,000 points instead of 7 million!). To be seen is the distribution of the x-component of the vorticity vector in a series of planes parallel to each other and all perpendicular to the main dimension of the configuration, the X-axis on the picture. Particularly conspicuous are both marginal vortices, which convect downstream without being too strong dissipated. This is attributable first to the quality of the grid (even on the second level!) and second to the low-velocity preconditioning. Also to be noted starboard (blade advancing side) is the vortex cast off from the inner rotor radius. Finally, since the actuator disc map sets source terms in all three space directions, a relatively strong shearing takes place between the upper and lower sides, which causes the coloured vorticity stripes all over the disc surface. Of course even sharper details would appear on the finest level, as it has been checked with computations using the ONERAactuator disc map.

Figures 11 and 12 intend to show that discriminating two different rotors is possible. Two simulations on the second grid level were done first with the ONERAactuator disc map and second with the S4 map. Surface pressures on the top centreline are displayed in 11 and clearly exhibit differences even on the nose of the fuselage. The rotor signatures appear unmistakably on the tail boom and on the fin. The distribution of the x-component of the vorticity vector in a plane located 84% of a rotor radius aft of the rotor centre is depicted in 12. (We draw the attention of the reader to the thin vertical line crossing both left marginal vortices: it has been traced back to a post-processing problem but unfortunately could not be corrected.) Again, a clear distinction can be made between both rotors: the marginal vortices look somewhat different, and the position of the inner vortex is swapped form right to left indicating the opposite rotation directions: counterclockwise for the S4 map and clockwise for the ONERAmap if considered from above. Finally, the author is aware that the vortices of the S4 map seem to have a stronger magnitude and to be convected a bit lower than the vortices of the ONERAmap, which could be raised as an objection. Furthermore they do not exhibit an unsymmetrical pattern as for the ONERAmap, thus not clearly discriminating between the advancing and retreating sides (only indicated by the inner vortex). Although care had been taken when designing the test-case with the S4 map, it will be once again checked in a future analysis whether similarity coefficients of both rotors are actually identical.

CPU-Efficiency

Last, a few words on CPU-efficieny. First, all computations of the present work were run on the NEC SX-5Be/16 used by DLR, the processors of which are twice as slower as the fastest marketed ones. An acceleration factor of two is here in principle possible. Second, the author used at the time of validation a personal FLOWer version, in which loop collapsing was not yet available for the cell-centred discretisation, which is now the case by the time of writing this article. This had the nasty consequence to drastically reduce vector lengths down to about 40, well under the usual value achieved by FLOWer for large cases. A factor three is here expected. Third, a more advanced vectorisation of the implicit DDADI integration of turbulence equations has been in the meantime achieved, thus leaving here also freedom for acceleration. Fourth, running FLOWer in parallel mode on four processors reduces turn-around times at least by a factor three.

With all constraints and restrictions mentioned above, running 4000 cycles on the Dauphin configuration on the finest level (7 million points) in sequential mode required about 120 CPU-hours. When all potential acceleration factors are taken into account, it seems realistic to carry out exactly the same run within only 6 to 12 wall clock-hours, which could be acceptable for production simulations in an industrial context.

Conclusion

The so-called *quasi-steady* approach to simulating the flow around a complete helicopter consists in modelling the actual rotors by means of actuator discs. The way retained at DLR to such a framework has been presented with special emphasis on the numerical implementation of actuator discs. Reviewing the course of the development allowed pointing to the necessity of the final source term technique. Two applications have been done so far: the BO-105 and the Dauphin 365N, the latter of which made it even possible to capture the vorticity field.

Future activities will concentrate on further validation of the actuator disc feature, especially in switching more and more from the Dauphin configuration to the BO-105 one. Then both main and tail rotors will be accounted for in using Chimera grids, thus allowing greater flexibility in positioning and orienting disc surfaces. In addition, the newly developed automatic Cartesian background grid generator of FLOWer, as presented in [32], will be used in order to prevent scattering unnecessary points down to far-field boundaries. Care will also be taken to strive to the expected promising run-times.

Acknowledgements

The author feels very indebted to Joël Brézillon for countless friendly discussions on the Dauphin configuration: be it on the mesh, on his own results or generally on fuselage/rotor interactional aerodynamics. The author thanks also Berend van der Wall for his help in coupling S4 to FLOWer. Finally the author acknowledges gratefully the help of Walid Khier in providing the BO-105 mesh.

References

(References are listed in chronological order.)

[1] **W. Z. Stepniewski**
Rotary-Wing Aerodynamics, Volume 1: Basic Theories of Rotor Aerodynamics (With Application to Helicopters)
NASA Contractor Report 3082, 1979

[2] **D. L. Whitfield, A. Jameson**
Three-Dimensional Euler Equation Simulation of Propeller-Wing Interaction in Transonic Flow
AIAA 83-0236, 21st Aerospace Sciences Meeting, January 83, Reno, Nevada

[3] **D. L. Whitfield, J. M. Janus**
Three-Dimensional Unsteady Euler Equations Solution Using Flux Vector Splitting
AIAA 84-1552, 17th Fluid Dynamics, Plasma Dynamics and Lasers Conference, June 84, Snowmass, Colorado

[4] **N. J. Yu, S. S. Samant, P. E. Rubbert**
Flow Prediction for Propfan Configurations Using Euler Equations
AIAA 84-1645, 17th Fluid Dynamics, Plasma Dynamics and Lasers Conference, June 84, Snowmass, Colorado

[5] **R. G. Rajagopalan, J. B. Fanucci**
Finite Difference Model for Vertical Axis Wind Turbines
Journal of Propulsion and Power, Vol. 1, Nr. 6, Nov.-Dec. 1985, pp. 432-436

[6] **B. van der Wall**
Analytic Formulation of Unsteady Profile Aerodynamics and its Application to Simulation of Rotors
DLR Technical Report FB 90-28, 1990

[7] **I. Fejtek, L. Roberts**
Navier-Stokes Computation of Wing/Rotor Interaction for a Tilt Rotor in Hover
AIAA 91-0707, 29th Aerospace Sciences Meeting, January 91, Reno, Nevada

[8] **R. G. Rajagopalan, S. R. Mathur**
Three Dimensional Analysis of a Rotor in Forward Flight
Proceedings, American Helicopter Society, 47th Annual Forum, Phoenix, AZ, May 1991

[9] **L. Zori, S. Mathur, R. Rajagopalan**
Three Dimensional Calculations of Rotor-Airframe Interaction in Forward Flight
Proceedings, American Helicopter Society, 48th Annual Forum, Washington, D.C., June 1992

[10] **G. J. Schipholt, N. Voogt, J. van Hengst**
Investigation of Methods for Modelling Propeller-Induced Flow Fields
AIAA 93-0874, 31st Aerospace Sciences Meeting, January 93, Reno, Nevada

[11] **P. Lötstedt**
Properties of a Propeller Model in the Stationary Euler Equations
Computational Fluid Dynamics, 1994, pp. 594-604

[12] **N. Kroll, R. Radespiel, C. Rossow**
Accurate and Efficient Flow Solvers for 3D Applications on Structured Meshes
Lecture Notes of the Von Karman Institute for Fluid Dynamics, March 1994

[13] **M. S. Chaffin, J. D. Berry**
Navier-Stokes Simulation of a Rotor Using a Distributed Pressure Disk Method
Proceedings, American Helicopter Society, 51st Annual Forum, Fort Worth, TX, May 1995

[14] **R. Radespiel, N. Kroll**
Accurate Flux Vector Splittings for Schocks and Shear Layers
Journal of Computational Physics, 121, pp. 66-78, 1995

[15] **B. Eisfeld, H.-M. Bleecke, N. Kroll, H. Ritzdorf**
Structured Grid Solvers II: Parallelization of Block Structured Flow Solvers
AGARD Report R-807, October 1995

[16] **N. Hariharan, L. N. Sankar, J. Russell, P. Chen**
Numerical Simulation of the Fuselage-Rotor Interaction Phenomenon
AIAA 96-0672, 34th Aerospace Sciences Meeting, January 96, Reno, Nevada

[17] **R. Heinrich, K. Pahlke, H. Bleecke**
A Three-Dimensional Dual-Time Stepping Method for the Solution of the Unsteady Navier-Stokes Equations
Proceedings of the Conference on Unsteady Aerodynamics, July 17-18th, 1996, London, UK

[18] **W. G. Joo, T. P. Hynes**
The Simulation of Turbomachinery Blade Rows in Asymmetric Flow Using Actuator Disks
ASME, Journal of Turbomachinery, October 1997, Vol. 119, pp. 723-732

[19] **E. Turkel, R. Radespiel, N. Kroll**
Assessment of Preconditioning Methods for Multidimensional Aerodynamics
Computers and Fluids, Vol. 26, No. 6, pp. 613-634, 1997

[20] **D. D. Boyd, Jr., R. W. Barnwell**
Rotor-Fuselage Interactional Aerodynamics: An Unsteady Rotor Model
Proceedings, American Helicopter Society, 54th Annual Forum, Washington, D.C., May 1998

[21] **N. Bettschart**
Rotor Fuselage Interaction: Euler and Navier-Stokes Computations with an Actuator Disk
Proceedings, American Helicopter Society, 55th Annual Forum, Montreal (Canada), May 1999

[22] **R. Wilhelm**
Development and Testing of an Actuator Disk Boundary Condition Based on the DLR FLOWer Code
DLR Technical Report IB 129-99/22, Braunschweig 1999

[23] **S. Kim, S. Yang, D. Lee, S. Baftalovski, V. Makarov**
Three-Dimensional Flow Calculation Around/Through Isolated Nacelle with an Actuator Disk Modelling
35th AIAA/ASME/SAE/ASEE Joint Propulsion Conference and Exhibit, 20-24 June 1999, CA, Los Angeles

[24] **U. Reisch**
Simulation of Lattice Wings With the Actuator Disc Concept
DLR Technical Report IB 129-2000/13, Braunschweig 2000

[25] **V. Couaillier, P. Eliasson, J. Faßbender**
Enhancing Robustness for Advanced Turbulence Models in the European Project AVTAC
AIAA 2000-2407, Fluids 2000, June 2000, Denver, CO

[26] **J. Brézillon**
Simulation of Rotor-Fuselage Interactions by Using an Actuator Disk
Proceedings of the 26th European Rotorcraft Forum, The Hague, The Netherlands, September 2000

[27] **T. Schwarz**
Development of a Wall Treatment for Navier-Stokes Computations Using the Overset-Grid Technique
Proceedings of the 26th European Rotorcraft Forum, The Hague, The Netherlands, September 2000

[28] **P. Reynier**
Coupling Between an Actuator Disk and a Navier-Stokes Solver: Application to a Missile With Lattice Wings
DLR Technical Report IB 129-2001/12, Braunschweig 2001

[29] **H. Tadghighi**
Simulation of Rotor-Body Interactional Aerodynamics: An Unsteady Rotor Source Distributed Disk Model
Proceedings, American Helicopter Society, 57th Annual Forum, Washington, D.C., May 2001

[30] **W. Khier, F. Le Chuiton, T. Schwarz**
Navier-Stokes Analysis of the Helicopter Rotor-Fuselage Interference in Forward Flight
CEAS Aerospace Aerodynamics Research Conference, June 2002, Cambridge, UK

[31] **J. Sidès, K. Pahlke**
Progress Towards the CFD Computation of the Complete Helicopter: Recent Results Obtained by Research Centers in the Framework of the French-German CHANCE Project
CEAS Aerospace Aerodynamics Research Conference, June 2002, Cambridge, UK

[32] **N. Kroll, C. Rossow, D. Schwamborn, K. Becker, G. Heller**
MEGAFLOW – A Numerical Flow Simulation Tool for Transport Aircraft Design
ICAS 2002 Congress

Figures

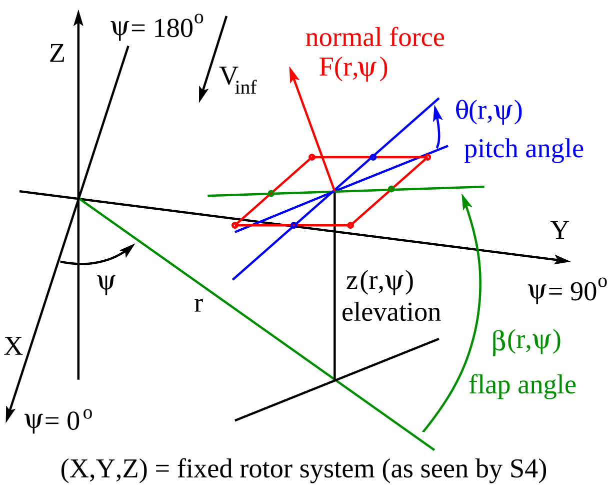

Figure 1: Blade element definition

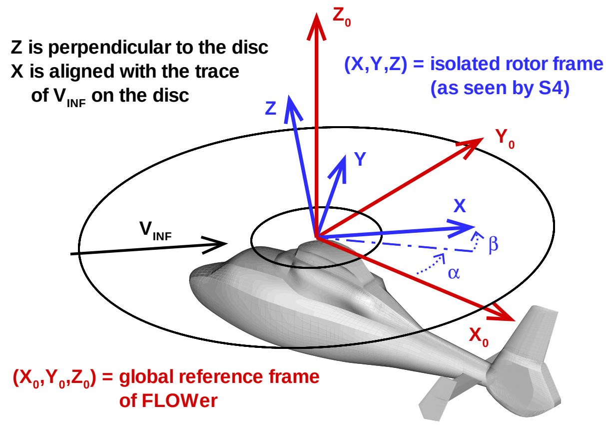

Figure 2: Reference frame definition

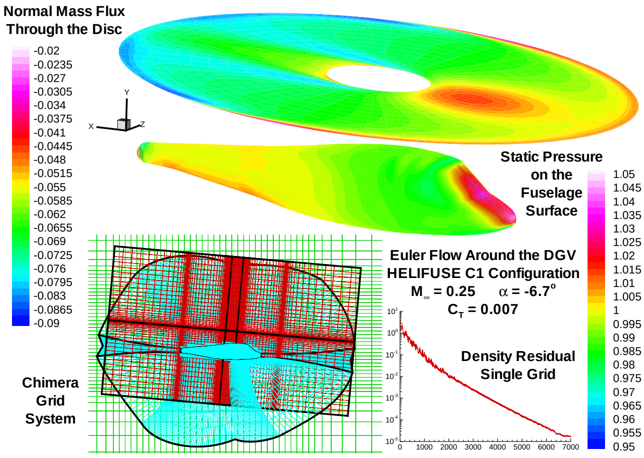

Figure 3: Chimera demonstration run

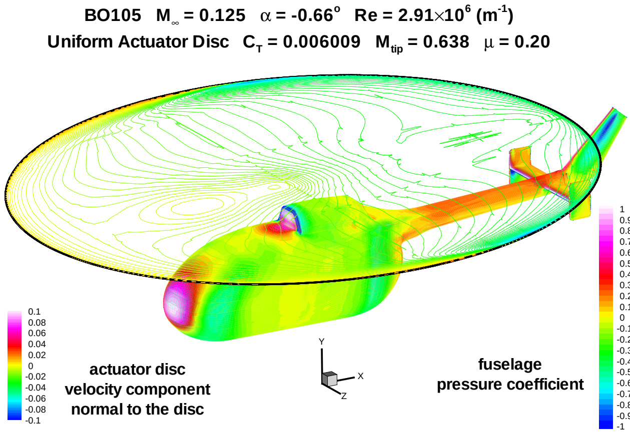

Figure 6: BO105 – Pressure coefficient distribution

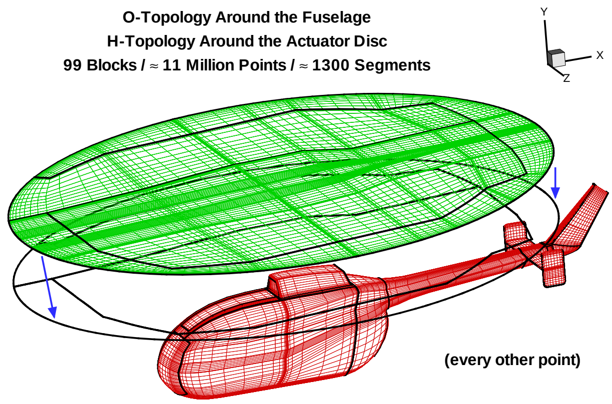

Figure 4: BO105 – grid level 2

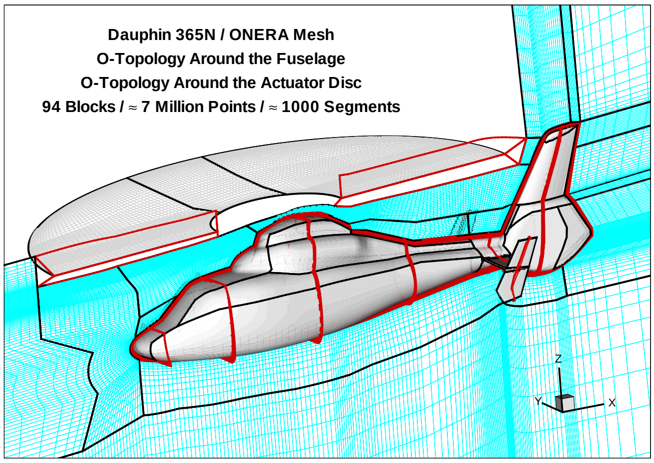

Figure 7: Dauphin 365N – grid level 1

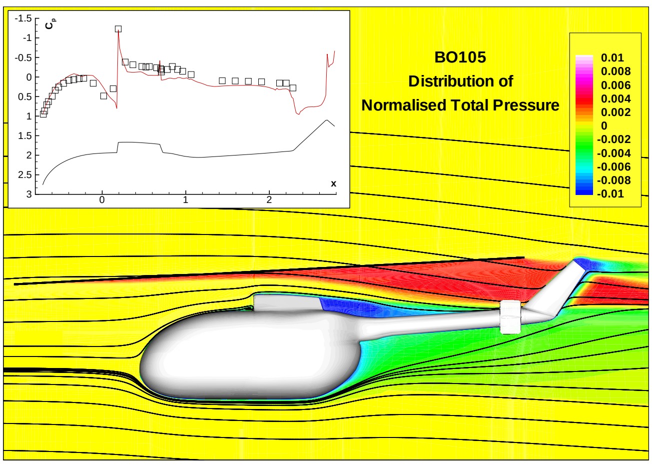

Figure 5: BO105 – Normalised total pressure distribution

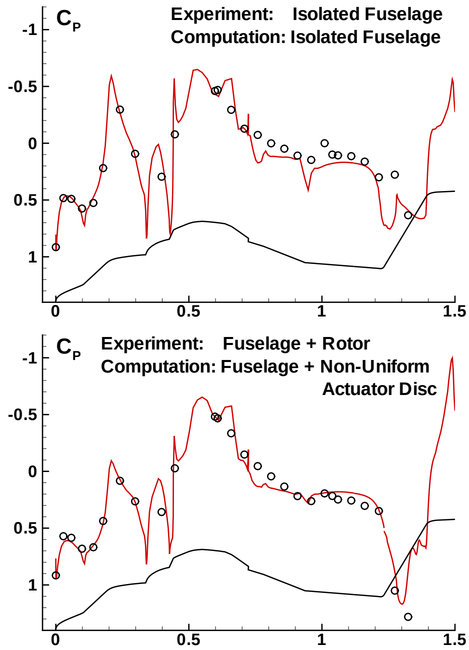

Figure 8: Dauphin 365N – Comparison simulation (solid lines) vs experiment (hollow circles) / pressures on the top centreline

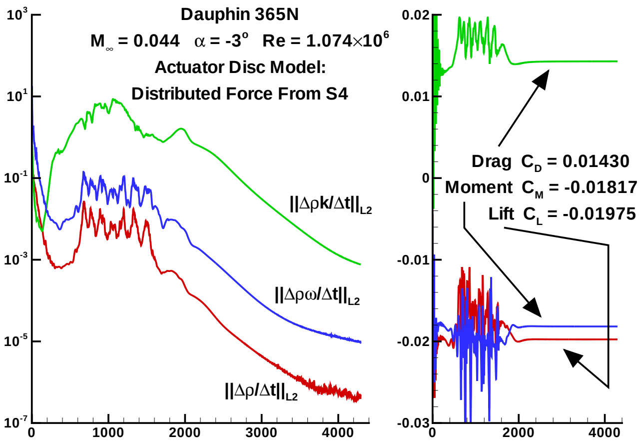

Figure 9: Dauphin 365N – Residual and coefficient convergence histories

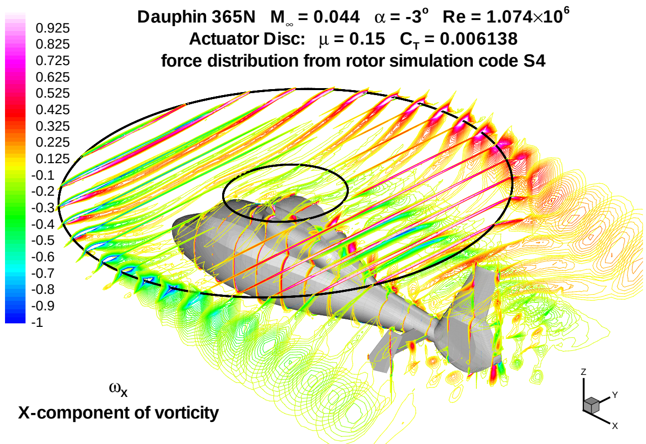

Figure 10: Dauphin 365N – Distribution of the X-component of vorticity

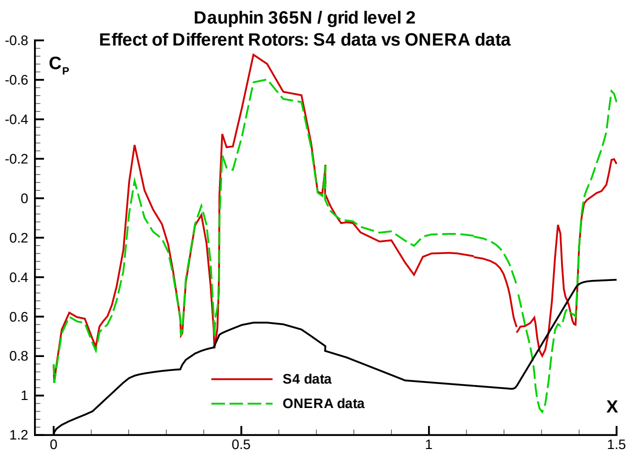

Figure 11: Dauphin 365N – Effect of different rotors: S4 data versus ONERA data – pressure on the top centreline

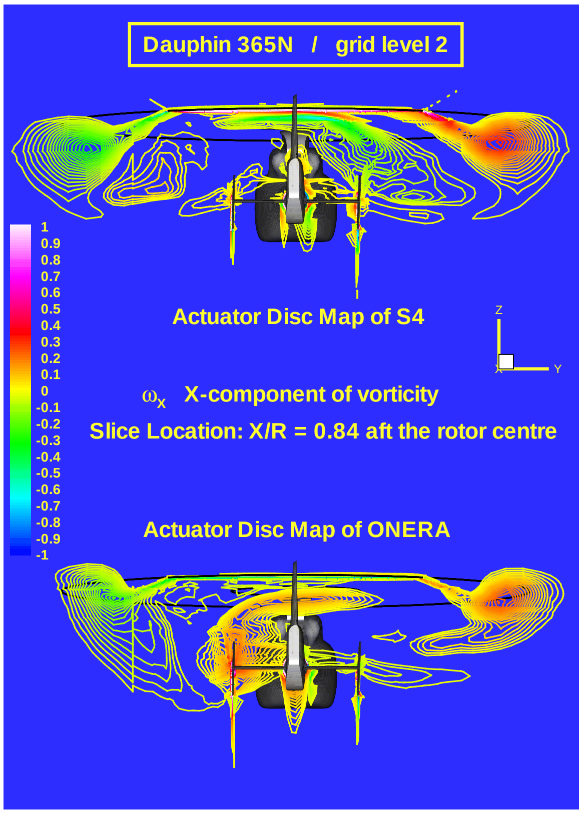

Figure 12: Dauphin 365N – Effect of different rotors: S4 map versus ONERA map – vorticity aft the rotor centre